Bulletin of the Seismological Society of America, Vol. 103, No. 3, pp. 2142–2150, June 2013, doi: 10.1785/0120120290

Short Note

Sequential H-κ Stacking to Obtain Accurate Crustal Thicknesses beneath Sedimentary Basins

by William L. Yeck,* Anne F. Sheehan,* and Vera Schulte-Pelkum*

Abstract Low-velocity sedimentary basins introduce error in many standard receiver-function (RF) analysis techniques including common conversion point (Dueker and Sheehan, 1997) and crustal thickness-V_P/V_S ratio (H-κ) stacking (Zhu and Kanamori, 2000). We describe a simple RF analysis method for obtaining accurate crustal thickness below seismic stations located in sedimentary basins. The method extends the methods of Zhu and Kanamori (2000). It employs an iterative two-layer depth-V_P/V_S stacking approach that first characterizes sediment properties (thickness and V_P/V_S) allowing for the accurate interpretation of Moho conversions. Without accounting for sedimentary layers, standard-RF analysis can mischaracterize crustal thickness based on Ps-phase delay by >10 km beneath deep basins. We test the technique with synthetic seismograms and with data from US Array Transportable Array (TA) stations from regions with sediment thicknesses that are well determined through other means. We find sequential H-κ stacking for sediment properties to be a simple technique that can benefit many RF-analysis studies and can play an important role in crustal seismic studies in areas with thick or variable sediments.

Introduction

The receiver-function (RF) technique is a well-established method that utilizes seismic P–S-converted waves to map out subsurface interfaces beneath a seismic receiver (Vinnik, 1977; Langston, 1979; Owens *et al.*, 1984). The presence of low-velocity sedimentary basins causes a delay of arrivals from deeper converters such as the crust–mantle boundary (Moho), which leads to incorrect mapping of the Moho to greater depth if the sediment layer is not accounted for. Reverberating phases in the sediment layer (referred to as multiples throughout here) may also overprint Moho arrivals (see Zelt and Ellis, 1998, for a detailed discussion on the effects of sediment on RFs). These complexities make it difficult to resolve Moho depth in sediment-affected RFs. Many techniques have been developed to accommodate these complexities, including the comparison with synthetic RFs (Sheehan *et al.*, 1995) and the use of *a priori* sediment information to perform wave-field continuation (Langston, 2011). Other techniques use laterally varying velocity models to account for average crustal velocity changes that can be caused by basins, for example, the use of the Crust 2.0 velocity model in the Earth Scope Automated Receiver Survey (EARS; Crotwell and Owens, 2005). In this note we show a simple and robust alternative, the characterization of both sediment and basement crustal properties through sequential two-layer H-κ stacking.

H-κ stacking (Zhu and Kanamori, 2000) employs a grid search through thickness (H) and V_P/V_S (compressional to shear velocity ratio, also denoted as κ) space in an effort to maximize the amplitude of stacked arrivals $s(H,\kappa)$ given by

$$s(H,\kappa) = w_1 \times \mathrm{RFS}(t_{Ps}) + w_2 \times \mathrm{RFS}(t_{PpPs}) - w_3 \times \mathrm{RFS}(t_{PsPs+PpSs}), \quad (1)$$

where w is weight value (all one in this note), t is the calculated time of the corresponding arrival (direct Ps phase and reverberated $PpPs$ and $PsPs + PpSs$ phases, where upper- and lowercase letters denote downgoing and upgoing rays, respectively) given an H-κ pair, and RFs is the receiver-function time series. The method works well in the case of a simple crust, but in the presence of sedimentary basins it overestimates crustal thickness by an amount roughly equal to the basin thickness (Fig. 1), where crustal thickness refers to the full basin + basement portion of the crust (surface to Moho; Fig. 2). This is the result of the delayed arrival of subbasin converted phases as they pass through seismically slow sediment. The delay of the Moho Ps phase can have an even larger

*Also at Cooperative Institute for Research in Environmental Sciences, University of Colorado, Boulder, Colorado 80309

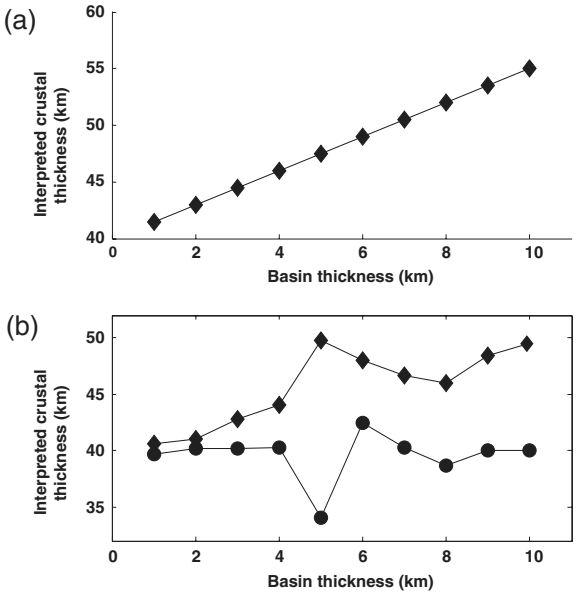

Figure 1. (a) The interpreted crustal thickness for 40-km-thick crust in the presence of sedimentary basins calculated using time-to-depth conversion based upon Moho *Ps* phase without accounting for basin effects. (b) Synthetic results from one-layer (diamonds) and two-layer sequential (circles) H-κ stacks for 40-km-thick crust. Synthetic RFs and an example velocity model are shown in Figure 2. One-layer H-κ stacks overestimate crustal thickness by an amount roughly equal to sediment thickness. Both methods fail when sediment reverberations are coeval with direct Moho *Ps* conversion (in this example at 5-km basin thickness).

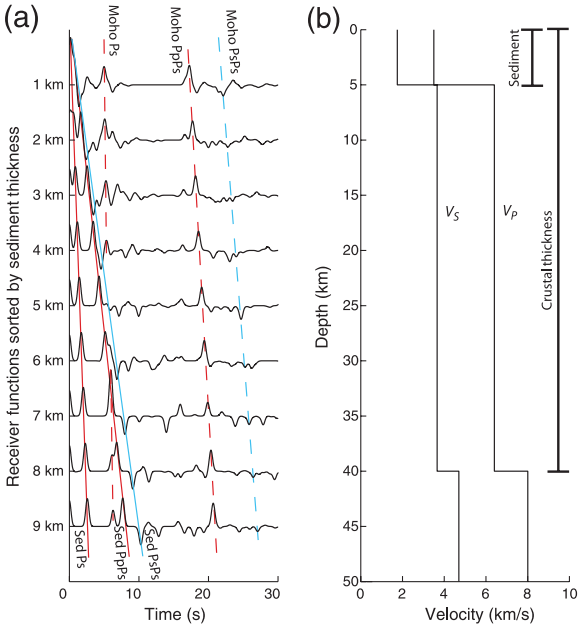

Figure 2. (a) Synthetic receiver functions calculated for a suite of sedimentary basin thicknesses. Synthetics shown were created using a slowness of 0.04 degrees/s. Sediment arrivals are indicated by solid lines, Moho arrivals dashed. Some small arrivals in receiver functions are artifacts from time-domain deconvolution. (b) An example velocity model used to create synthetics. Basin thicknesses were varied whereas crustal thickness remained constant.

effect on inferred Moho depth in methods that rely solely on this phase to characterize crustal thickness. Furthermore, the coeval arrival of reverberating basin phases with the Moho *Ps* phase complicates interpretation. We find that through a sequential two-layer H-κ stacking routine it is possible to remove timing-delay effects introduced by sediments as well as characterize reverberating sediment phases to ensure that these phases are not interpreted as Moho signal. Tang *et al.* (2008) examined H-κ stacking for a generic three-layer crust; the technique presented here focuses on characterizing a sedimentary layer and removing its effect from Moho-depth estimates.

Method

In our method we first perform an H-κ stack to constrain basin properties, then use the basin results as *a priori* information when stacking for deeper seismic discontinuities. In order to perform a two-layer H-κ stack, we create two suites of RFs from the data, each with unique frequency content. Deconvolution is performed in the time domain (Ligoria and Ammon, 1999). High-frequency RFs are used when stacking for sediment properties. For the sedimentary layer we have found the best results with RFs created using a Gaussian pulse width of 0.75 s, corresponding to a Gaussian filter parameter a of 5 (pulse width in seconds $= 5/3\sqrt{a}$). Although high-frequency RFs are typically noisier than long-period RFs, they resolve shallow features better and allow for higher resolution H-κ stacks, as pulse widths are narrower and the amplitudes of sediment arrivals are larger (Fig. 3). Lower frequency RFs created using a Gaussian pulse width of 1.18 s (Gaussian filter parameter of 2) are used when stacking for Moho depth. Both suites of RFs are independently quality controlled by (1) applying a minimum signal-to-noise criterion (>5) of the first *P* arrival on the predeconvolution vertical component; (2) applying a minimum variance reduction

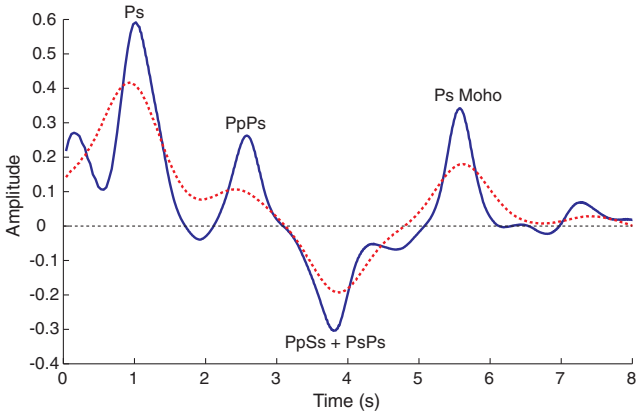

Figure 3. Average moveout corrected RFs for TA station G22A in the Powder River Basin computed using Gaussian pulse width parameter $a = 5$ (0.75-s Gaussian pulse; blue) and $a = 2$ (1.18-s Gaussian pulse; red dashed). Notice that the initial large pulse, often referred to as a delayed sediment direct *P* in low frequency RFs, is clearly a sediment *Ps* conversion in the high-frequency RF.

Table 1
Synthetic H-κ Stack Results

Model Sediment Thickness (km)	Crustal Thickness (One-Layer H-κ stack)	Crustal V_P/V_S (One-Layer H-κ stack)	Sediment Thickness (Two-Layer H-κ stack)	Sediment V_P/V_S(Two-Layer H-κ stack)	Crustal Thickness (Two-Layer H-κ stack)	Basement V_P/V_S (Two-Layer H-κ stack)
1	40.6	1.77	0.9	2.61	39.7	1.74
2	41.9	1.76	1.8	2.31	40.2	1.73
3	42.8	1.77	2.9	2.10	40.2	1.73
4	44.1	1.76	4	2.01	40.3	1.73
5	49.8	1.52	5	1.96	34.1	1.65
6	48	1.65	6	2.01	42.5	1.74
7	46.7	1.9	7	2.01	40.3	1.73
8	46	1.81	7.9	2.03	38.7	1.87
9	48.4	1.81	9	2.00	40	1.75

of the final RF criterion (Ligorria and Ammon, 1999). We applied a minimum variance reduction of 90% for low-frequency RFs and 70% for high-frequency RFs (due to their noisier nature).

When stacking, we first create basin H-κ stacks. The main difference between our basin H-κ stacks and typical Moho H-κ stacks is the use of higher frequencies. Next, a Moho H-κ stack is performed using time adjustments from the sediment layer determined in the first step. The sequential nature of our method occurs during the Moho H-κ stack and lies in the adjustment of the predicted timing of the Moho Ps, $PpPs$, and $PsPs + PpSs$ phases when accounting for the previously acquired sediment properties. The timing adjustments of respective phase arrivals are simply

$$t_{Ps} = (H - h_1) \times \left(\sqrt{\frac{1}{V_{2s}^2} - p^2} - \sqrt{\frac{1}{V_{2p}^2} - p^2} \right) + h_1 \times \left(\sqrt{\frac{1}{V_{1s}^2} - p^2} - \sqrt{\frac{1}{V_{1p}^2} - p^2} \right), \quad (2)$$

$$t_{PpPs} = (H - h_1) \times \left(\sqrt{\frac{1}{V_{2s}^2} - p^2} + \sqrt{\frac{1}{V_{2p}^2} - p^2} \right) + h_1 \times \left(\sqrt{\frac{1}{V_{1s}^2} - p^2} + \sqrt{\frac{1}{V_{1p}^2} - p^2} \right), \quad (3)$$

and

$$t_{PsPs+PpSs} = 2(H - h_1) \times \left(\sqrt{\frac{1}{V_{2s}^2} - p^2} \right) + 2h_1 \times \left(\sqrt{\frac{1}{V_{1s}^2} - p^2} \right), \quad (4)$$

where h_1 is sediment thickness from the first H-κ stack, V_{1p} and V_{2p} are the respective assumed sediment and sub-sediment crust P velocities, V_{2s} is the subcrust S velocity calculated from the current grid-search κ value, V_{1s} is the sediment S velocity calculated from the previous H-κ stack, p is slowness and H is the current grid-search value for total crustal thickness (i.e., surface to Moho distance). Using these time adjustments, the resulting H-κ stack is corrected for sediment delay effects. It is essential to check to see if the Moho Ps phase arrival is coeval with either the sediment $PpPs$ or $PsPs$ phases. If this is the case, standard RF analysis techniques breakdown and more rigorous approaches, such as wave-field continuation and decomposition (Langston, 2011), are needed.

We have found sequential H-κ stacking has many benefits over simultaneous stacking for both layers. First, sequential stacking is computationally much faster than stacking for both layer properties simultaneously. H-κ stacking relies on an exhaustive grid search and therefore increasing the parameter space greatly increases processing time. Second, simultaneous stacking would require stacking RFs of distinct frequency content, possibly necessitating the use of further weighting parameters as the amplitudes of each frequency suite are unique.

Synthetic Example

We tested the method using synthetic seismograms created using the reflectivity code RESPKNT developed by Randall (1994). Synthetic seismograms were created for a suite of layered crustal models with variable sediment thicknesses (Fig. 2). Crustal and sediment properties that remained constant include a sediment V_P of 3.5 km/s, sediment V_P/V_S of 2, crustal thickness of 40 km, and crustal V_P and V_P/V_S of 6.4 and 1.75 km/s, respectively. The H-κ grid search was performed through a sediment-thickness range of 0–12 km and V_P/V_S range of 1.7–2.7, crustal thickness range of 30–50 km and V_P/V_S range of 1.65–2.1 with a grid spacing of 0.1 and 0.01 for H and V_P/V_S, respectively. Table 1 displays two-layer H-κ stacking results. Basin thickness is well determined in all cases, but basin V_P/V_S is poorly constrained with basin thicknesses less than 2 km due to the nearly simultaneous arrival of all three phases. In this range V_P/V_S has a much smaller effect on constraining sediment thickness (Fig. 4). Crustal thickness is well determined in all cases except for sediment thicknesses from ~5 to 7 km. In this range

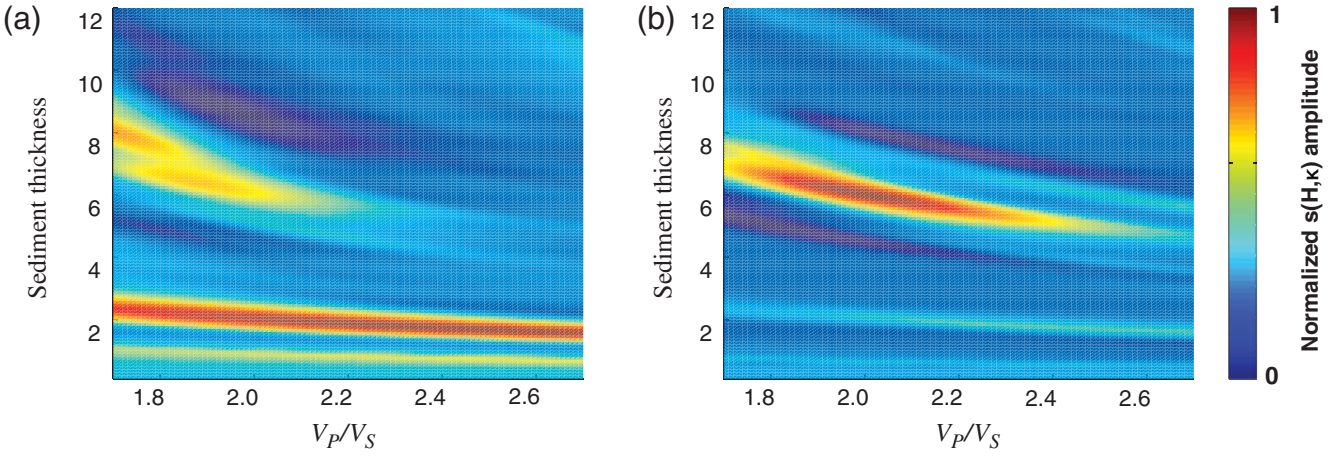

Figure 4. H-κ grid search results for sedimentary layer parameters, utilizing synthetic seismograms as shown in Figure 2. (a) Sediment layer H-κ stack for synthetic seismogram with sediment layer of 2 km. (b) Sediment layer H-κ stack for synthetic seismogram with sediment layer of 6 km. At low sediment thicknesses, as in the 2-km-thickness case (a), V_P/V_S is difficult to constrain as seen in the nondiscrete maxima (red line at 3–2 km spread along the V_P/V_S axis). In thicker sediments (case b), maxima become more discrete.

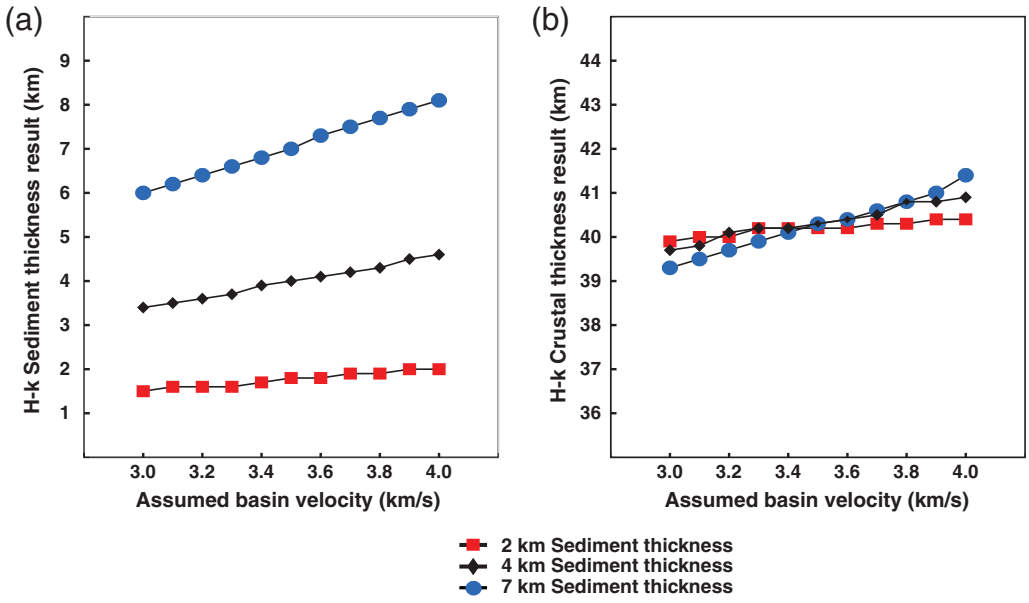

Figure 5. (a) Synthetic sediment thickness H-κ stack results as a function of assumed sediment V_P. Synthetics were created using sediment V_P of 3.5 km/s, basement V_P of 6.4 km/s, and crustal thickness of 40 km. Larger errors occur in deeper basins, with a 2-km difference in sediment thickness for 1 km/s difference in assumed sediment V_P in the case of a 7-km-deep basin. (b) The selected crustal thicknesses for the same two-layer H-κ stacks. Errors in sediment thickness propagate nearly equally to crustal thickness results.

the direct Moho *Ps* phase coincides with the reverberated sediment phases. This emphasizes the need to check that the direct crustal *Ps* phase does not overlap with sediment reverberations.

In order to accurately determine layer thicknesses, H-κ stacking relies on a prior assumption of the layer's average velocity (Zhu and Kanamori, 2000). To accurately constrain sediment thickness it is important to choose an accurate sedimentary layer V_P (Fig. 5). The error due to inaccurate selection of sediment V_P has a nearly equal effect on the offset of results for both crustal thickness and sediment thickness, though crustal thickness errors due to inaccurate sediment V_P are relatively small compared with errors due to choosing an inaccurate crustal V_P (~0.5 km per 0.1 km/s error; Zhu and Kanamori, 2000; Fig. 5).

Data Examples

We selected two basins in which to demonstrate the method, the Powder River Basin area and the Denver Basin.

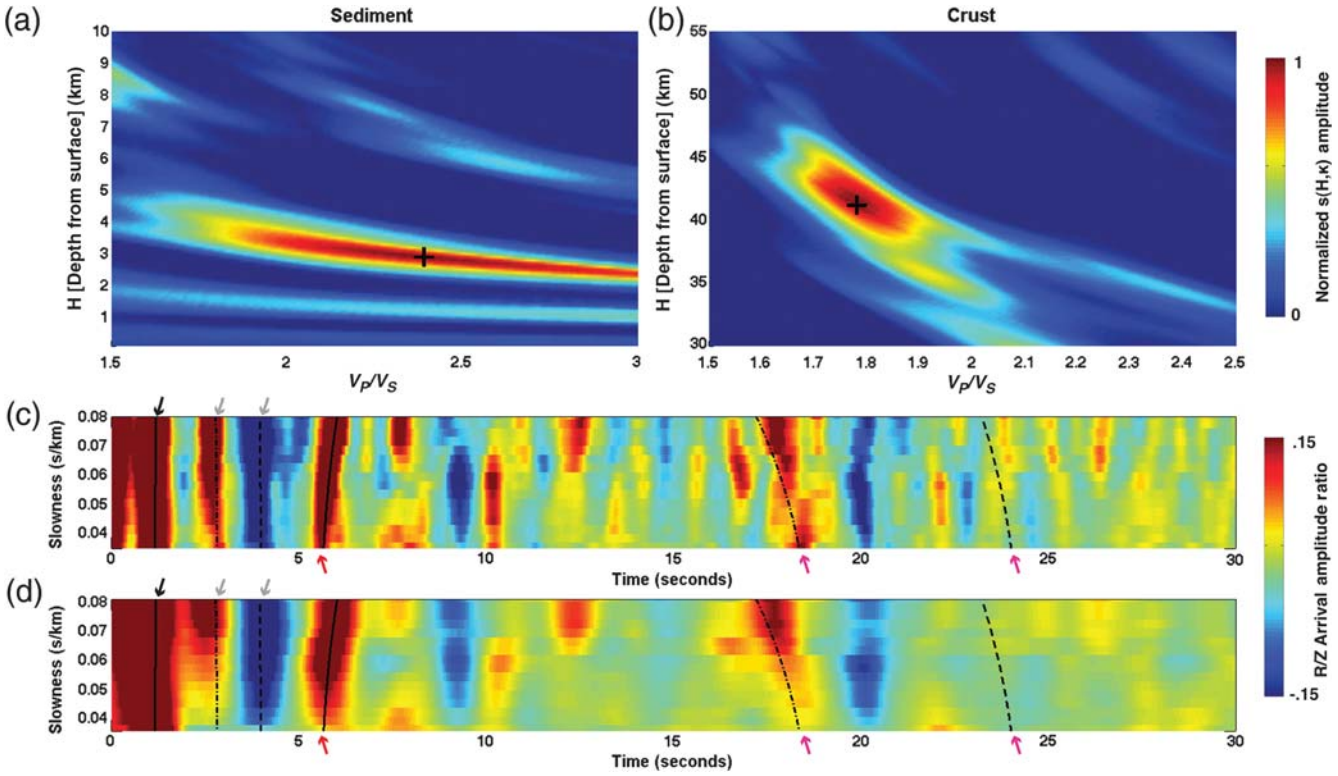

Figure 6. Two-layer H-κ stacking results for USArray station G22A in the northern part of the Powder River Basin in Montana. Both sediment thickness (a) and crustal thickness (b) are well constrained. Sediment arrivals are seen clearly in high-frequency receiver function moveout plot (c) and marked by solid (Ps), dash-dotted ($PpPs$), and dashed ($PsPs + PpSs$) lines (r = radial, v = vertical). (d) Moveout plot for low-frequency receiver functions. Black, gray, red, and pink arrows denote sediment Ps, sediment multiples, Moho Ps, and Moho multiples, respectively.

The Powder River Basin proves to be an ideal area in which to utilize sequential stacking. The velocity structure of the Denver Basin has unusual effects on sediment-multiple amplitudes, but our method nevertheless recovers the correct sediment thickness when compared with constraints derived from well logs. Events with magnitude $m_b > 5.1$ and epicentral distance from 28–99 degrees were used in the RF calculations. Event traces remained at their original 40-Hz sample rate and were filtered with a 0.03–10 Hz Butterworth bandpass filter. RFs were calculated using iterative time-domain deconvolution with 200 iterations (Ligorria and Ammon, 1999).

Powder River Basin

The Powder River Basin situated in northern Wyoming shows clear stackable sedimentary multiples. As an example we use a north–south transect of USArray TA stations through the Powder River Basin (stations F22A, G22A, H22A, and I22A). Stations F22A and G22A are at the northern end of the basin, H22A is centered in the basin, and I22A is situated in the basin's foredeep. For H-κ stacking, we selected an average sediment V_P of 3.6 km/s from well logs (Moore, 1985) and an average basement V_P of 6.7 km/s from nearby active source seismic studies (Snelson *et al.*, 1998). Figure 6 shows an example sequential stack for station G22A. The comparison of moveout plots from the two suites of RFs shows that higher frequencies are necessary to resolve sediment structure. Results for all stations are listed in Table 2. Basement V_P/V_S listed refer to that of solely the basement layer. Sediment thickness, crustal thickness, and crustal V_P/V_S are all well constrained. As in the synthetic examples, sediment V_P/V_S is poorly constrained. All stations show clear sedimentary arrivals that follow expected moveout (Fig. 7). Sediment thickness agrees with the expected geometry of thickness increasing towards the basin's foredeep (station I22A). At stations H22A and I22A the Moho Ps arrival is obfuscated by sediment multiples, making crustal stacks unreliable for these stations (Fig. 7). In the case of station H22A, the picked Moho (black line) is roughly 1 s after what appears to be a weak Moho signal, near the negative sediment reverberation. In the case of station I22A, the Moho Ps arrival and sediment multiples are coeval. Figure 7 demonstrates how with this method it is straightforward to ascertain whether sediment reverberations interfere with the Moho Ps arrivals.

Denver Basin

The velocity structure of the Denver Basin has effects on amplitudes of multiples and requires care in stacking.

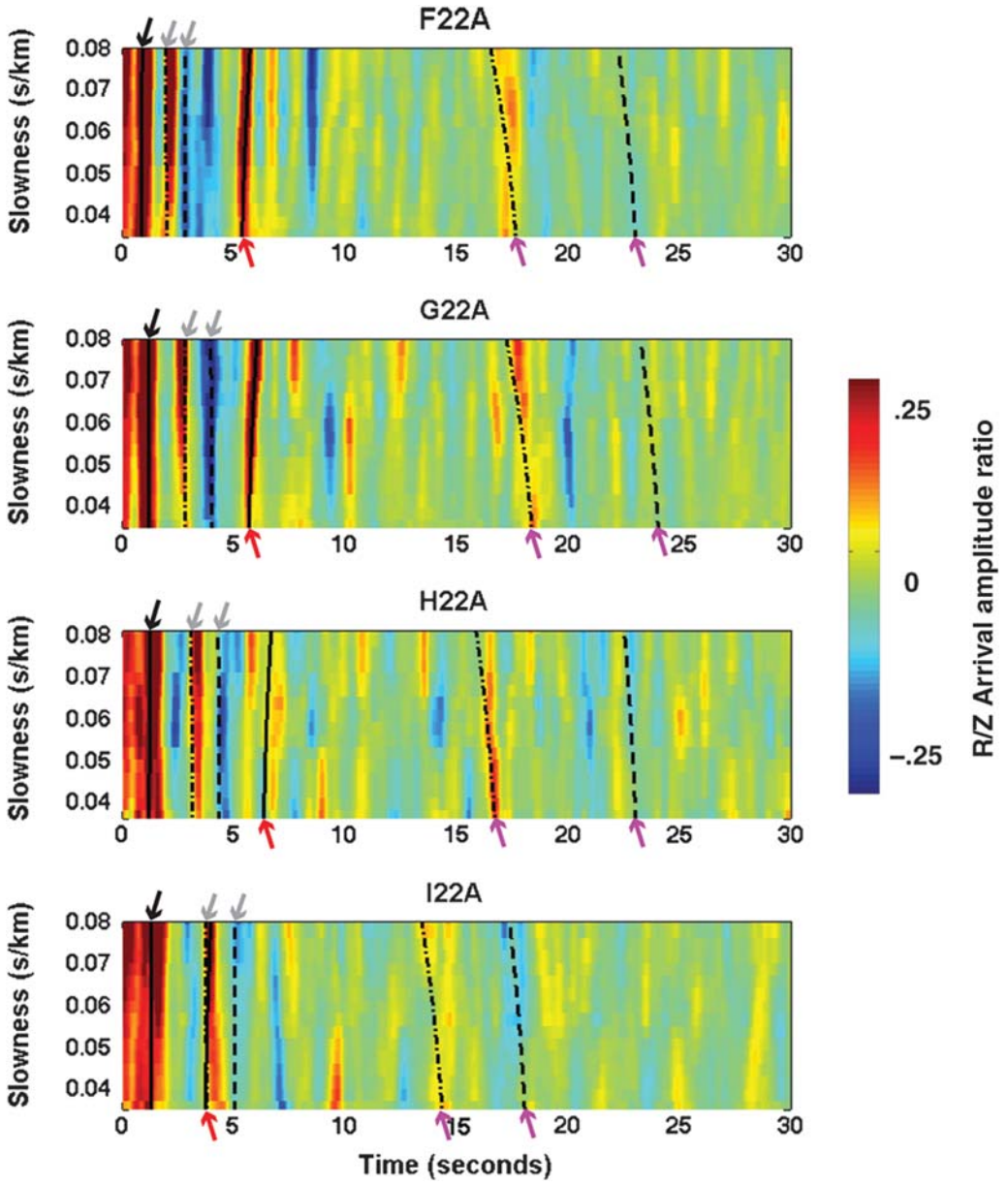

Figure 7. Moveout plots of high-frequency receiver functions for TA stations F22A, G22A, H22A, and I22A (r = radial, v = vertical) in the Powder River Basin. Predicted moveout curves based on H-κ stack results for phase arrivals are denoted with arrows and lines with: black arrows and solid lines for sediment Ps; gray arrows and dashed lines for sediment multiples; red arrows and solid lines for Moho Ps; pink arrows and dashed lines for Moho multiples.

We selected USArray TA stations P24A, P25A, P26A, and P27A, starting at the western edge of the Denver Basin, the foredeep of the basin, and ending 200 km east. A crustal V_P of 6.4 km/s was selected for the H-κ stack based on a nearly collocated previous active source experiment through the Denver Basin (Prodehl and Lipman, 1989). Sediment V_P values of 3 and 4 km/s were separately assumed as these values are poorly constrained. Using a range of sediment V_P gives an allowable range of crustal thicknesses that result from variability in the velocity structure of the basin. In the Denver Basin we only observe direct Ps and $PsPs$+$PpSs$ phases (Fig. 8). The lack of a clear $PpPs$ is likely due to a specific combination of V_P, V_S, and density contrasts; it is not easily reproduced with forward modeling and we have insufficient data (particularly on V_S and density) to model this distinct characteristic. However, the method still provides sediment constraints that agree with independent estimates (Hemborg, 1996). Table 2 shows results for both two-layer stacks and single-layer H-κ stacks. Bootstrap errors are for the most part reduced when a sediment layer is taken into account in stacking (Table 2). Stack results for P25A are shown in Figure 8. Taking sediment into account in the stacking changes the interpretation of crustal geometry (Fig. 9). In the case of station P24A, in the deepest portion of

Table 2
Crustal Thickness Single and Two-Layer H-κ Stack Results for Transportable Array Stations

Station	Assumed Sediment Velocity (km/s)	Assumed Basement Velocity (km/s)	Sediment Thickness (Two-Layer H-κ stack)	Sediment V_P/V_S (Two-Layer H-κ stack)	Crustal Thickness (Two-Layer H-κ stack)	Basement V_P/V_S (Two-Layer H-κ stack)	Crustal Thickness (One-Layer H-κ stack)	Crustal V_P/V_S (One-Layer H-κ stack)
F22A	3.6	6.7	2.1 ± 0.08	2.54 ± 0.07	40.5 ± 0.61	1.77 ± 0.02	42.6 ± 1.04	1.83 ± 0.03
G22A	3.6	6.7	2.9 ± 0.13	2.39 ± 0.13	41.2 ± 0.96	1.78 ± 0.02	44.4 ± 1.97	1.83 ± 0.06
*H22A	3.6	6.7	3.7 ± 0.11	2.22 ± 0.08	32.7 ± 4.38	2.17 ± 0.20	35.4 ± 5.99	2.21 ± 0.42
*I22A	3.6	6.7	4.7 ± 0.23	2.02 ± 0.17	32.7 ± 0.97	1.57 ± 0.03	37.3 ± 7.51	1.66 ± 0.07
P24A	3.0	6.4	4.2 ± 0.65	1.69 ± 0.35	37.0 ± 3.82	2.06 ± 0.11	42.0 ± 6.16	1.98 ± 0.31
P25A	3.0	6.4	3.7 ± 0.19	1.83 ± 0.06	41.0 ± 3.66	1.95 ± 0.13	45.6 ± 5.83	1.91 ± 0.17
P26A	3.0	6.4	2.7 ± 0.17	2.17 ± 0.13	40.3 ± 4.31	1.86 ± 0.12	43.8 ± 4.42	1.89 ± 0.11
P27A	3.0	6.4	2.1 ± 0.08	2.01 ± 0.07	45.5 ± 1.67	1.67 ± 0.03	48.1 ± 1.33	1.69 ± 0.003
P24A	4.0	6.4	5.7 ± 0.90	1.66 ± 0.36	38.4 ± 4.02	2.07 ± 0.11	42.0 ± 6.16	1.98 ± 0.31
P25A	4.0	6.4	4.9 ± 0.23	1.83 ± 0.05	42.5 ± 3.30	1.93 ± 0.12	45.6 ± 5.83	1.91 ± 0.17
P26A	4.0	6.4	3.4 ± 0.21	2.26 ± 0.12	41.4 ± 4.51	1.85 ± 0.13	43.8 ± 4.42	1.89 ± 0.11
P27A	4.0	6.4	2.8 ± 0.08	2.01 ± 0.07	46.0 ± 1.34	1.67 ± 0.03	48.1 ± 1.33	1.69 ± 0.003

*Stations where Moho Ps phase is obfuscated by sediment multiples. Crustal thickness and V_P/V_S values reported to demonstrate method results but do not accurately represent the Earth due to this obfuscation.

the basement, crustal thickness changes by 4.4 km between the one-layer and two-layer H-κ stacking methods. Sediment results correlate well with local basement structural maps (Hemborg, 1996), with a better fit when 3 km/s sediment V_P is assumed (Fig. 9). Our single-layer H-κ stack results are similar to EARS results (Crotwell and Owens, 2005) except in the case of station P24A; however, crustal thicknesses decrease when the sediment layer is accounted for (two-layer H-κ stack), as compared to both one-layer H-κ stacks and EARS crustal thickness estimates (Fig. 9). Accounting for sediment properties results in a shallower Moho, although relative variations in Moho geometry are largely the same.

Discussion and Conclusion

The effects of sedimentary basins on RFs can cause significant bias when interpreting crustal thickness. Through a simple two-layer H-κ stack it is possible to constrain basin

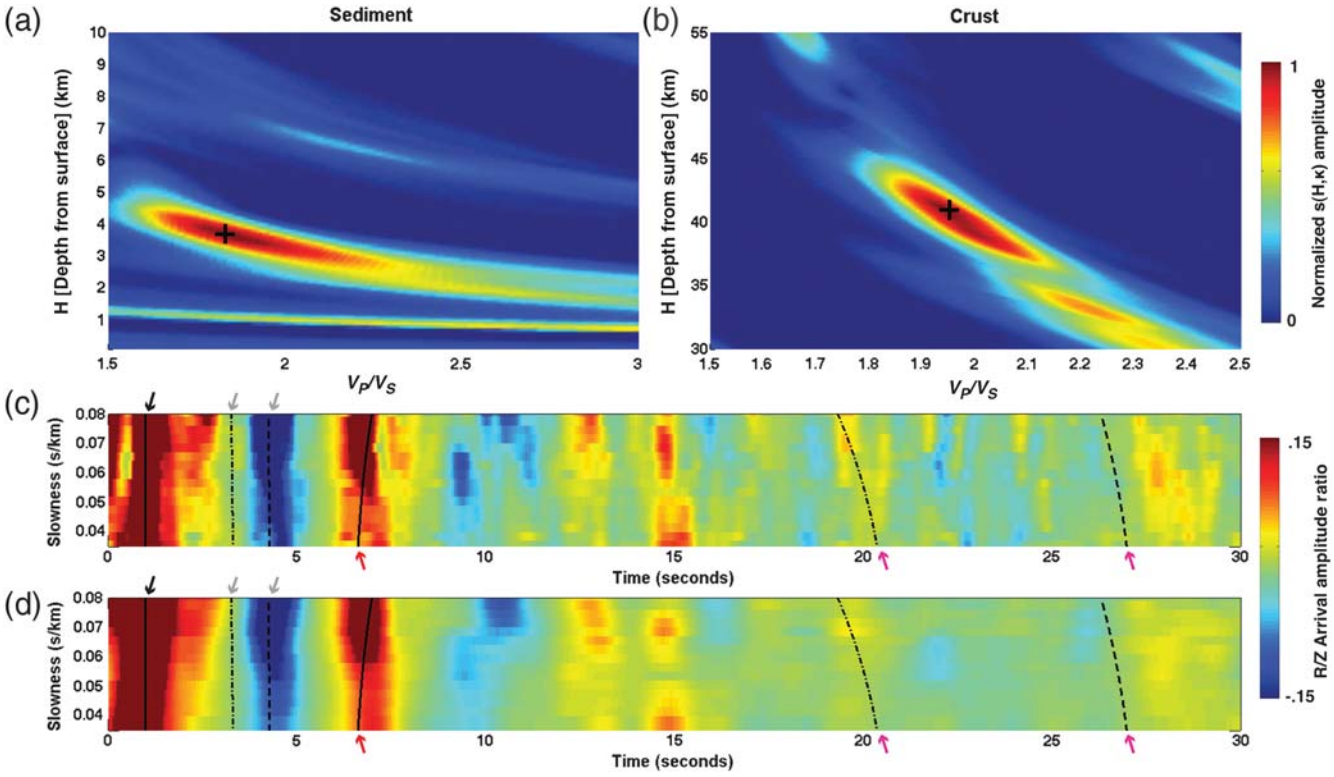

Figure 8. Two-Layer H-κ stacking results for USArray station P25A in the Denver Basin near Deer Trail, Colorado. See Figure 6 description.

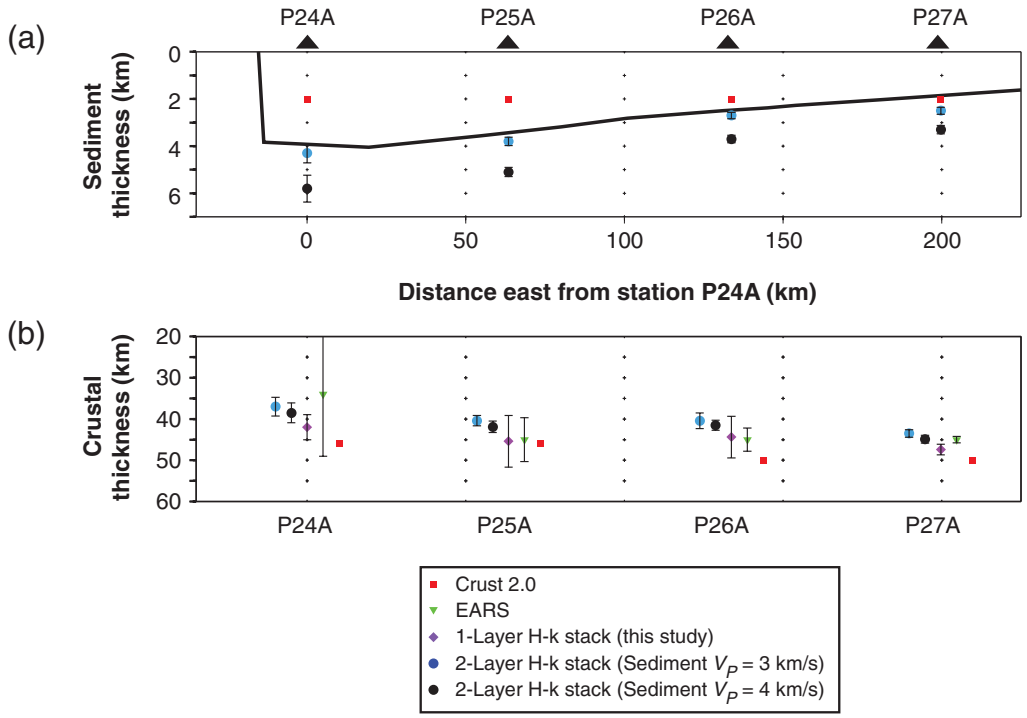

Figure 9. (a) Sediment thickness from west to east across Denver Basin including results from two-layer H-κ stack assuming sediment V_P of 3 km/s (blue circles) and 4 km/s (black circles), Crust 2.0 (red squares), and basement-structure map from Hemborg (1996) (black line). The two-layer H-κ stack with sediment $V_P = 3$ km/s provides an excellent fit to the basement map. (b) Crustal thickness from two-layer H-κ stacking results above (blue and black circles), single-layer H-κ stack (purple diamonds), EARS (green triangles), and Crust 2.0 (red squares). Note the reduced error with two-layer H-κ stack (blue and black circles).

properties and correct for their effects, though the technique is limited to cases where the Moho *Ps* and sediment reverberations are not coincident in time; in the latter case, our method identifies locations where standard H-κ stacks will also fail. The method assumes a simple basin and crustal structure and may fail in cases where basins have larger complexity (e.g., multiple large velocity contrasts between sediment packages). It is therefore essential that the user does not blindly utilize this method without interpreting the waveforms. Still, this technique serves as a simple method for constraining sediment properties and therefore reducing error due to basin signals. These easily obtained basin constraints not only can benefit H-κ stacking for crustal thickness but also can be used to improve the accuracy of other RF-analysis techniques such as Common Conversion Point stacking.

Data and Resources

The facilities of the Incorporated Research Institutions for Seismology Data Management System (IRIS DMS), and specifically the IRIS Data Management Center, were used for access to waveform and metadata required in this study. The IRIS DMS is funded through the National Science Foundation (NSF) and specifically the GEO Directorate through the Instrumentation and Facilities Program of the National Science Foundation (NSF) under Cooperative Agreement EAR-1063471. Data from the TA network were made freely available as part of the EarthScope USArray facility, operated by IRIS and supported by the NSF, under Cooperative Agreements EAR-0323309, EAR-0323311, EAR-0733069. This work was supported by the NSF Grant EAR-0843657.

Acknowledgments

We thank IRIS and PASSCAL for providing easy access of TA seismic data, Karen Fischer for discussions on receiver functions in sediments, and Anton Dainty and Jordi Julià for constructive comments.

References

Crotwell, H., and T. Owens (2005). Automated receiver function processing, *Seismol. Res.Lett.* **76,** no. 6, 702–709.

Dueker, K., and A. Sheehan (1997). Mantle discontinuity structure from midpoint stacks of converted *P* to *S* waves across the Yellowstone hotspot track, *J. Geophys. Res.* **102,** 8313–8327.

Hemborg, H. T. (1996). Basement structure map of Colorado with major oil and gas fields, *Colorado Geological Survey Map Series 30*, scale 1:1,000,000.

Langston, C. A. (1979). Structure under Mount Rainier, Washington, inferred from teleseismic body waves, *J. Geophys. Res.* **84,** 4749–4762.

Langston, C. A. (2011). Wave-field continuation and decomposition for passive seismic imaging under deep unconsolidated sediments, *Bull. Seismol. Soc. Am.* **101,** no. 5, 2176–2190.

Ligorria, J., and C. Ammon (1999). Iterative deconvolution and receiver-function estimation, *Bull. Seismol. Soc. Am.* **89,** no. 5, 1395–1400.

Moore, W. R. (1985). Seismic profiles of the Powder River basin, Wyoming, in *Seismic Exploration of the Rocky Mountain Region*, R. R. Griesand

and R. C. Dyer (Editors), Rocky Mountain Association of Geologists and Denver Geophysical Society, Denver, Colorado, 187–200.

Owens, T. J., G. Zandt, and S. R. Taylor (1984). Seismic evidence for an ancient rift beneath the Cumberland Plateau, Tennessee: A detailed analysis of broadband teleseismic *P* waveforms, *J. Geophys. Res.* **89,** 7783–7795.

Prodehl, C., and P. W. Lipman (1989). Crustal structure of the Rocky Mountain region, in *Geophysical Framework of the Continental United States*, L. C. Pakiser and W. D. Mooney (Editors), Geological Society of America Memoir, Boulder, Colorado, 249–284.

Randall, G. (1994). Efficient calculation of complete differential seismograms for laterally homogeneous earth models, *Geophys. J. Int.* **118,** 245–254.

Sheehan, A. F., G. A. Abers, C. H. Jones, and A. L. Lerner-Lam (1995). Crustal thickness variations across the Colorado Rocky Mountains from teleseismic receiver functions, *J. Geophys. Res.* **100,** 20,391–20,404.

Snelson, C., T. Henstock, G. Keller, K. Miller, and A. Levander (1998). Crustal and uppermost mantle structure along the deep probe seismic profile, *Rocky Mountain Geol.* **33,** no. 2, 181–198.

Tang, C., C. Chen, and T. Teng (2008). Receiver functions for three-layer media, *Pure Appl. Geophys.* **165,** no. 7, 1249–1262.

Vinnik, L. (1977). Detection of waves converted from *P* to *SV* in the mantle, *Phys. Earth Planet. In.* **15,** 39–45.

Zelt, B. C., and R. M. Ellis (1998). Receiver function studies in the Trans-Hudson orogen, Saskatchewan, *Can. J. Earth Sci.* **36,** 585–603.

Zhu, L., and H. Kanamori (2000). Moho depth variation in southern California from teleseismic receiver functions, *J. Geophys. Res.* **105,** 2969–2980.

Department of Geological Sciences
University of Colorado
Boulder, Colorado 80309

Manuscript received 24 September 2012